Int J Adv Manuf Technol (2015) 77:15–26
DOI 10.1007/s00170-014-6363-9

ORIGINAL ARTICLE

Cross-wedge rolling of a 4Cr9Si2 hollow valve: explorative experiment and finite element simulation

Hongchao Ji · Jinping Liu · Baoyu Wang · Zhenhua Zheng · Jianghua Huang · Zhenghuan Hu

Received: 27 May 2014 / Accepted: 8 September 2014 / Published online: 10 October 2014

Abstract Cross-wedge rolling (CWR) has many advantages in the production of shafts and rolling while a hollow valve is widely used in engine production. In this study, we use the CWR process to produce a hollow valve made of 4Cr9Si2 steel and present the experimental results. To evaluate the CWR process and deeply understand the deformation characteristics, a 3D finite element model (FEM) of the CWR process is established, and the mechanism of material flow, the temperature distribution, and the strain and rolling force are analyzed. The following conclusions are drawn based on the experiments and numerical simulations: changing the stretching angle (β) can effectively avoid swollen holes; the forming quality of the workpiece can be greatly improved when the forming angle (α) is equal to 35° and the stretching angle (β) is equal to 5° and 4° in the knifing and stretching zones, respectively; the CWR process is an effective technique to manufacture hollow valves for industrial production.

Keywords Cross-wedge rolling · Hollow valve · Small diameter · 4Cr9Si2 · Stretching angle

1 Introduction

The valve is an important auto engine component that is responsible for air intake and gas exhaust. With the development of automotive technology, the demand for hollow valves has increased. Two methods are used to produce hollow valves: drilling into a solid valve and reverse extrusion. However, these methods have many disadvantages, such as low material utilization, low production efficiency, and high cost. Therefore, an advanced manufacturing technology for hollow valve production must be explored. Cross-wedge rolling (CWR) is a plastic forming process, in which cylindrical workpieces are deformed into axisymmetric stepped parts using two or more wedge tools that move along the tangent direction of the workpieces. The process is conducted at an elevated temperature to acquire relatively low deformation forces. CWR possesses the following advantages: high production efficiency, low material cost, and high material utilization rate [1, 2]. Shu et al. [3–5] used the finite element (FE) software DEFORM to analyze the multiwedge CWR (MCWR) process. The rolling process of the MCWR for a railway vehicle axle was simulated, and the regularities of metal flow and stress distribution were analyzed in detail. Pater et al. [6–8] studied the CWR process. The distributions of the strain, stress, strain rate, and temperature of the workpiece and the tool forces were numerically investigated. Li and Lovell [9–12] established a simplified model of the flat CWR and analyzed the stress and deformation of workpieces. Zhou et al. [13–16] studied the connecting rod through CWR, analyzed workpiece bending, and investigated the changes in workpiece stress and temperature during the CWR process. The characteristics of each bending stage were clearly classified, and the bending mechanisms were identified. The study established the basic ideas to solve bending.

A number of studies have been carried out on the CWR processes for hollow shaft production. Pater and Bartnicki [17, 18] studied the three-roll CWR without a mandrel forming the hollow shafts and analyzed the parameters of the CWR process through numerical simulation. The plate wedge rolling of hollow shafts was also comparatively analyzed. Lovell et al. [19, 20] studied CWR theory and technology for hollow shaft parts. Experiments and FE simulation were performed to

H. Ji · J. Liu (✉) · B. Wang · Z. Zheng · J. Huang · Z. Hu
School of Mechanical Engineering, University of Science and Technology Beijing, No. 30 Xueyuan Road, Haidian District, 100083 Beijing, China
e-mail: liujp@ustb.edu.cn

J. Liu
e-mail: jhustb13@gmail.com

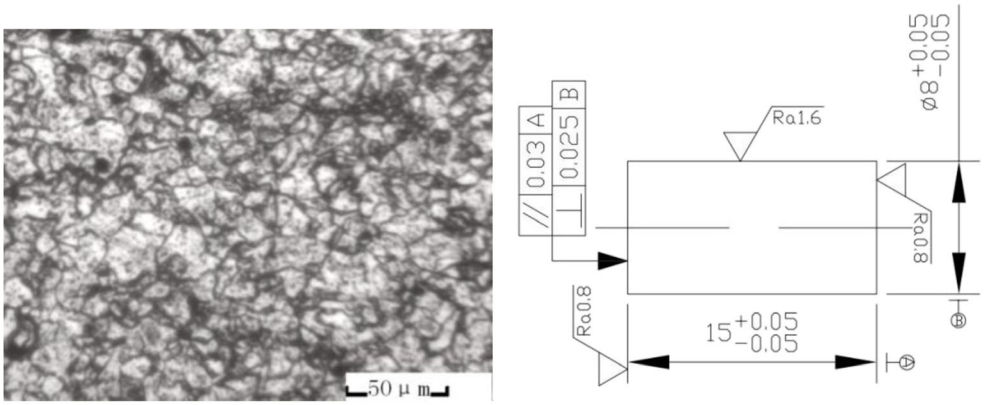

Fig. 1 **a** Grain size of 4Cr9Si2 after annealing; **b** test specimen size

study the unstable conditions when flattening hollow shaft CWR plate pieces. Du et al. [20–23] studied the deformation characteristics of hollow shafts, which they then compared with those produced with and without mandrel rolling. The study also explored microstructure evolution and phase transformation during the CWR process. Wang et al. [24, 25] identified and investigated the process parameters of CWR via the FE method and deduced the influential role of these parameters on the quality of rolled hollow shafts.

Most CWR-related studies only focus on low-alloy steel, with few of these studies exploring heat resistance. In the present study, we use CWR to produce a typical hollow valve. 4Cr9Si2 steel is a martensitic steel that is widely used in industrial production. Compared with low-alloy steel, 4Cr9Si2 steel has many advantages, such as lower plasticity, higher shrinkage rate, and higher sensitivity to temperature. However, the production of hollow valves, especially those with small diameters, is considerably difficult. Compared with hollow valves with a large diameter, hollow valves with a small diameter are likely to break in the CWR process. These hollow valves also suffer from other defects during the CWR process, e.g., swollen, in which the hole within the wedge is enlarged. Changing the stretching angle (β) could solve this problem. In this work, experiments are conducted to study the different effects of the CWR process parameters on the forming process and to achieve good forming quality. We use the FE software DEFORM to determine the material flow mechanism, the temperature distribution, and the strain and rolling force.

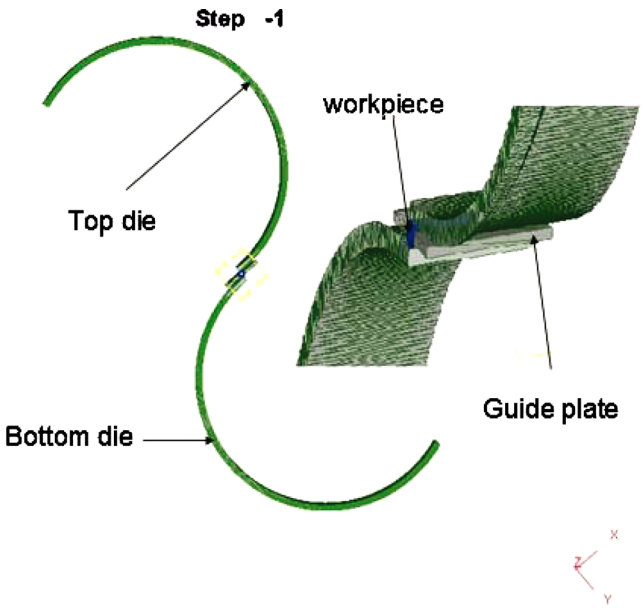

Fig. 2 Geometry mode for DEFORM

2 Finite element modeling (FEM) and experiments

2.1 Determining material constitutive relation

The structure and chemistry of metal materials are influenced by deformation factors such as velocity, temperature, and timing. The Arrhenius equation is widely used to describe the relationship among flow stress, strain rate, and temperature under high-temperature conditions [25–28]. The effects of temperature and strain rate on deformation behavior can be represented by the Z parameter in an exponential type equation. 4Cr9Si2 is very sensitive during deformation in different temperatures and strain rates. The CWR process is characterized by large deformation. In this work, we used the Kumar model to describe the following constitutive relation:

$$\dot{\varepsilon} = A[\sinh(\alpha\sigma)]^n \exp(-Q/RT) \quad (1)$$

where A (s^{-1}) and (MPa^{-1}) are the material constants, n is a constant closely related to the strain rate, σ is flow stress, R is the universal gas constant, ε is the strain rate (s^{-1}), T is the deformation temperature in Kelvin, and Q is the activation energy of deformation (J/mol).

The chemical compositions (wt%) of 4Cr9Si2 are as follows: 0.4C–9Cr–3Si–1Mn–0.6Ni–(bal.) Fe. Figure 1a shows the grain size of 4Cr9Si2 after annealing. Cylindrical specimens with a diameter of 8 mm and a height of 15 mm were

Table 1 Parameter of cross-wedge rolling simulation

Parameter	Value
Speed of roll (rpm)	10
Workpiece temperature (°C)	1150
Tools temperature (°C)	20
Environment temperature (°C)	20
Heat transfer coefficient (W/m^2 K)	40×103
Convection coefficient (W/m^2 K)	20
Friction factor	1
Mesh number for billet	90,000
Tool material	H3
Billet material	4Cr9Si2
Billet diameter (d) (mm)	Φ11×5/6/7, Φ12×6
Billet length (L) (mm)	110

machined from the wrought billet, as shown in Fig. 1b. Hot compression tests were conducted on a Gleeble 1500 thermo mechanical simulator under the forming temperatures of 950, 1000 °C, 1050, and 1100 °C. The selected strain rates were 0.01, 0.1, 1, and 5 s^{-1}. The true stress–strain curve could then be obtained. The material constitutive relation was determined by linear regression. The equation is as follows:

$$\dot{\varepsilon} = e^{31.25}[\sinh(0.00758\sigma)]^{4.9535}\exp(-382980/RT) \quad (2)$$

2.2 Establishment of boundary conditions

Using Pro/E, we established the geometry for CWR, which we then saved as an .stl file after importing into DEFORM. The geometry model is shown in Fig. 2. The model consists of the roll, workpiece, and guide plate. Before establishing the FE model of CWR, the following assumptions were made:

1. Tools and guide plates are rigid. Given the negligible elastic deformation of tools and guide plates, two wedged tools and guide plates were considered as rigid models for the tool materials.

Table 2 The main technical parameters of H500

Parameter	Value
Roll speed (r min^{-1})	10/12/15
Motor power (kW)	36
Roll diameter (mm)	500
Roll width (mm)	450
The maximum diameter of the rolling (mm)	40
The maximum length of rolling (mm)	400

2. A billet is a plastic material model. In the forming process, a billet is characterized by large deformation, plastic deformation is large, and the amount of elastic deformation is small and can thus be disregarded.
3. A roll rotates at a fixed step size. In practical rolling, roll speed accelerates, remains constant, and then decelerates. The acceleration time is very short. In DEFORM, roll speed was set to 8 r/min according to an actual rolling H500 mill.
4. To maintain asymmetrical CWR and to reduce CPU processing time, only half of the model was simulated.
5. Friction coefficient was assumed to be constant in the whole CWR process regardless of the use of cooling water. The frictional force in the shear friction model is defined by:

$$\mathrm{fs} = m \times k \quad (3)$$

where *fs* is the frictional stress, *k* is the shear yield stress, and *m* is the friction factor. The friction factor between the workpiece and the tools was 1.0.

6. The following are the boundary conditions of heat transfer: the workpiece undergoes convection, radiation, and heat exchange with the environment. In the CWR process, workpiece temperature increases because of friction. Heat exchange in a workpiece is a highly complex process. The main factors of the heat exchange coefficient are interface temperature, heating time, and the actual contact area. These factors were combined with the field data and

Fig. 3 Experimental equipment

H500 mill

Electric Tube Furnace

Table 3 The main technical parameters of electric tube furnace

Parameter	Value
Power rating (kW)	4
Rated temperature (°C)	1200
Rated voltage (V)	220
Chamber size (mm)	Φ60×1000

numerical temperature conditions. The room temperature was 20 °C, and the workpiece and air convection coefficient was 20 W/m^2 K. The heat transfer coefficient between the workpiece and the mold set was 40×10^3 W/m^2 K [29–31].

The summary of the adopted simulation parameters of the CWR process is listed in Table 1.

2.3 Experimental tests

The experimental tests on the CWR process were conducted using the H500 mill and electric tube furnace at the University of Science and Technology Beijing in Beijing, China. The H500 mill and the electric tube furnace are shown in panels a and b of Fig. 3, respectively. The main technical parameters are listed in Table 2. The main technical characteristics are listed in Table 3. The experimental billets were provided by an auto parts company (Guangdong Huaiji) and included the A3, #45, and 4Cr9Si2 pipe material.

The experiment was divided into four groups. The calculation parameters are shown in Table 4.

4Cr9Si2 is the main material used for valves. In the CWR forging process, 4Cr9Si2 demonstrates many characteristics, including low plasticity, high shrinkage rate, and high sensitivity to temperature. Hole ovalization inevitably occurs in the production of hollow valves with a small diameter. However, the shrinkage status of the hole cannot be clearly determined. All these factors increase the difficulty of producing 4Cr9Si2 hollow valves by CWR.

The experimental parameters are based on previous research methods and numerical simulations. The optimum parameters of the hollow billet valve were determined by analyzing the effect of different parameters. Each experiment was performed with A3 steel initially. If the rolling process could be established, then the 4Cr9Si2 material was rolled. Several workpieces were rolled to maintain the stability of the rolling state.

Table 4 Main process parameters for simulation

Item	Forming angle α (°)	Stretching angle β (°)	Area reduction Ψ (%)
1	30, 35, 38, 40	5–4	65.9
2	35	4, 4.5–4, 5, 5–4, 6, 6.5–6	65.9
3	35	5–4	65.9
4	35	5–4	51, 59.5, 65.9

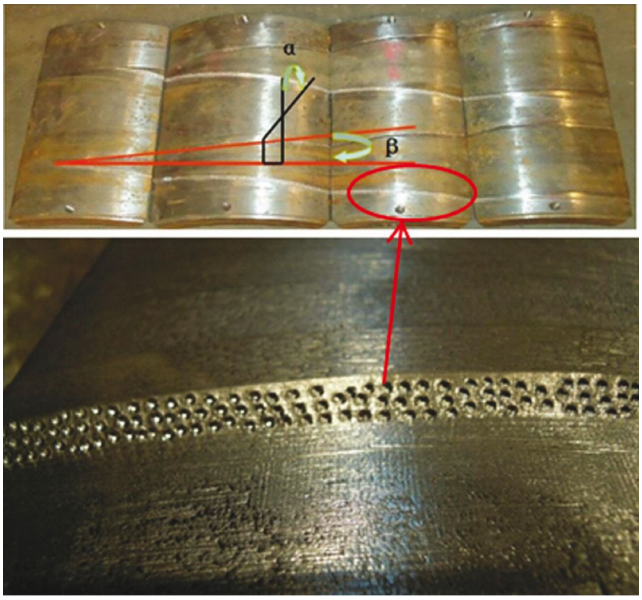

Fig. 4 The surface of mold

According to the experimental program for mold production, two processing parameters can be considered to save time and reduce experimental costs. All the molds satisfied the requirements of the experiment. The follow-up test was revised based on the primary processing. Dense dots were introduced to the wedge of each mold (as shown in Fig. 4) to increase friction. The length of the material was 110 mm. The workpiece was placed in the electric tube furnace and heated up to 1150 °C. Given the small size of the workpiece and the quick heat radiation, the workpiece was heated and transferred through a socket. This method effectively reduced the temperature of the workpiece. The workpiece was heated for complete austenitization, transferred quickly to the H500 mill, and then rolled. The quality of the rolled piece, including the surface quality, inner and outer diameters, geometrical shapes, and state of the inner surface, was checked after air cooling.

3 Results and discussion

3.1 Experimental results

In the CWR process for the production of 4Cr9Si2 hollow valves, several factors lead to ovalization, e.g., the small size of the valve structure, the mold chilling effect resulting from a decrease in the rolling surface temperature, and the large deformation resistance of 4Cr9Si2. Ovalization leads to roll rotation failure, roll breakage, and mold wear rolling defects. Therefore, this condition presents a challenging obstacle in the CWR

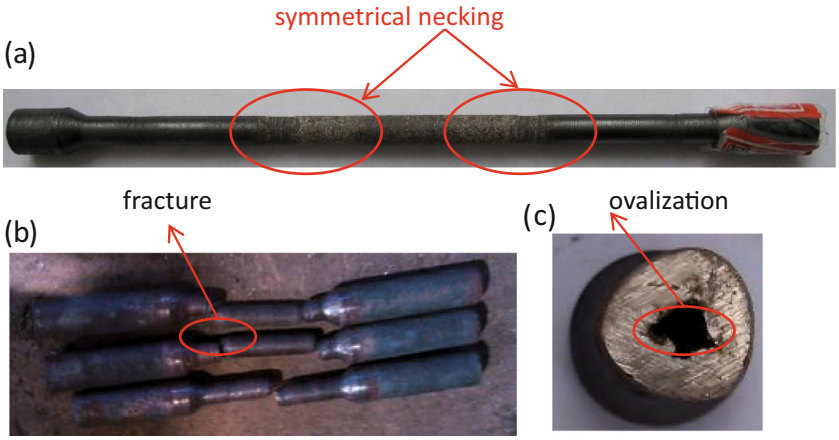

Fig. 5 Defects of rolled pieces

process. In this study, an experimental test was performed on the primary roll process parameters to determine the following major flaws: the oval hole and the swelling from the wedge. These defects were considered in modifying the parameters, mold structure, and other measures to achieve the basic product.

3.1.1 Serious ovalization of the rolled piece

While the mold wedges in the rolled piece and produces radial compression, transverse stretching occurs as a consequence of the blockade to the axial flow of the compressed metal. This condition leads to the ovalization of the rolled piece. A serious ovalization causes a range of issues, such as impeded rotation, rupture of the rolled piece, ovalization of the inner bore, and cracks in the inner wall.

In our experiment, we initially used a rolled piece made of carbon steel. Once the rolling course was established, the rolled stainless steel piece was tested. In this case, ovalization was caused mainly by the mismatches of the axial and lateral flows of the metal during the rolling attempt. The ovalization of the rolled 4Cr9Si2 piece and the other related defects were resolved by matching the forming angle with the stretching angle.

As shown in the Figs. 5a, b, the rolled 4Cr9Si2 piece is partly drawn down and ruptured. The blank used in the figure is Φ12×6. Under the same parameters, the rolled steel piece A3 does not show this phenomenon. Unlike carbon steel, 4Cr9Si2 has poor plasticity, low liquidity, and high deformation resistance. When the mold wedges into the rolled piece, the latter undergoes instant radial compression. With poor axial flow, the metal will flow laterally and become restricted radially by the mold, which leads to the ovalization of the rolled piece. As the rolling process reaches the stretching stage, the metal continues to undergo stacking and repeated rubbing. At this point, ovalization worsens, which can impede or even stop the rotation completely. In this case, the rolled piece is at risk of being drawn down or getting ruptured.

4Cr9Si2 is sensitive to temperature and has a narrow heat deformation temperature range. The surface cooling of the rolled piece increases because of heat loss through convection and chilling while its deformation resistance increases as plasticity and liquidity decrease. These conditions finally lead to the ovalization, drawing down, and rupture of the rolled piece. Small rolled pieces, such as those measuring Φ11×5/6/7 and Φ12×8, experience a major temperature drop and can hardly take shape. Therefore, heating temperature and time

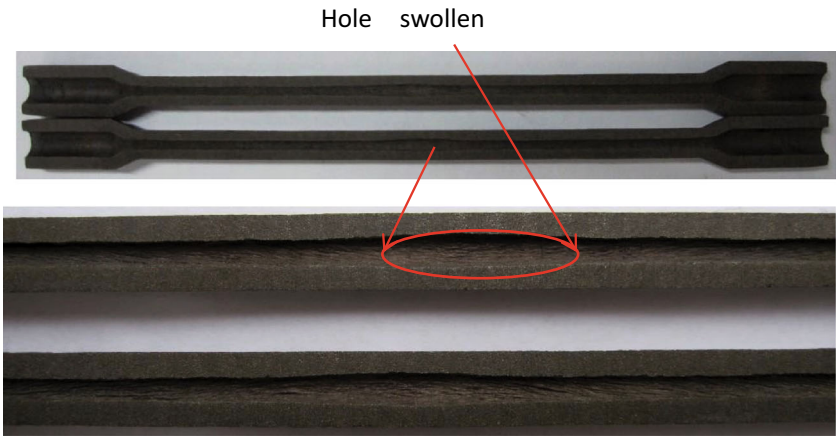

Fig. 6 The swollen hole after rolling

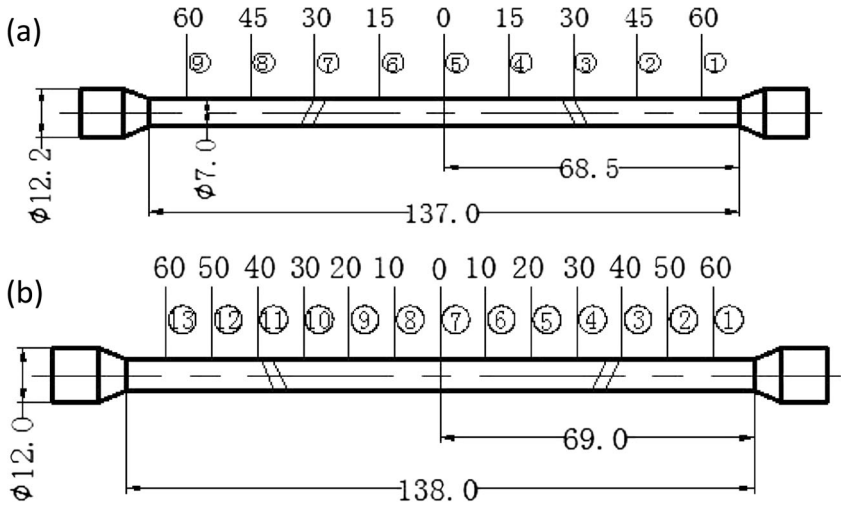

Fig. 7 Measured positions of rolled piece

has an important influence on the forming of rolled pieces in terms of preventing temperature drop. Appropriate heating temperature and time should be explored. In our experiment, tubular heating effectively reduced the temperature drop.

Figure 5c shows the cross section of the central plane of the rolled piece, which is triangular and shows serious ovalization. As mentioned previously, the mismatch between the axial and lateral flows in the 4Cr9Si2 hollow valve during the CWR process causes ovalization. Moreover, the inner surface of the rolled piece undergoes deformation during the rolling of the tube without a mandrel. With the radial compression and axial extension of the rolled piece, the inner bore continuously shrinks. Consequently, the metal surface in the deformation zone is repeatedly pressed into an oval or a triangle. The main defect is ovalization. The experiments in this work were performed by selecting the process parameters. After several rolling experiments, the following reasonable parameters were selected: forming angle α=35° and stretching angle at knifing zone β=5° and at stretching zone β=4° (the outer diameter is 7 mm, the inner diameter is 2.2 mm, and the surface is smooth).

3.1.2 Enlarged hole within the wedge

An enlargement of the inner bore of the wedge occurred in every rolled piece in the experiment. As shown in Fig. 6, the diameters of the inner bores on both sides of the central symmetry plane within the range of 15 mm are significantly large. The bore at which wedging was initiated shows the largest diameter. The diameters of the bores on both sides decrease gradually until the same diameter is reached. As seen from the profile, the edge line

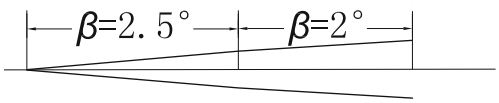

Fig. 8 The schematic of molds with change stretching angle

of the inner surface is arc-shaped. Consider a sectional measurement of the rolled piece with the following process parameters: forming angle of 35°, stretching angle of 4°, workpiece size of 12 mm×6 mm, and theoretical diameter after rolling of 7 mm. The measuring position is presented in Fig. 7a, which shows that the mean bore diameter on the central symmetry plane, that is, plane ⑤, is larger than that on planes ①②⑧⑨ by 0.6 mm. To obtain a product with a uniform internal diameter, we must process the inner bores, which incur high costs and material waste. Therefore, defects must be studied and addressed to solve the problem.

In this study, our mold was designed to have different stretching angles, as shown in Fig. 8. Hence, the stretching angles from the wedged-in section to the stretching section were set with different values. The parameters that could effectively solve the swollen holes problem were then selected, and the final effect was observed in the formation of the 4Cr9Si2 rolled piece:

When mold wedges into a rolled piece with a blow down on both sides, horizontal tensile stress is generated, and the inner bores at the initial wedged-in section is enlarged. In our experiment, the inner bore deformation was uncontrollable during the CWR of the hollow valve. Thus, we could only change the metal stress by changing the process parameters and reducing the enlargement of the inner bore, which were achieved by improving the metal flow condition. In the rolling experiment and numerical simulation, the axial flow velocity decreased as the stretching angle increased at a fixed forming angle. This condition favored the shrinkage of the inner bore on the central symmetry plane. Therefore, metal flow and lateral flow must match to avoid enlarged hole in the rolled piece while maintaining the uniform shrinkage of inner bores.

Condition 1: α=35°, stretching angle at the knifing zone β =4.5°, and stretching angle at the stretching zone β=4°. The hole shrinkage effect did not change significantly after forming.

Table 5 Outer and inner diameters in different positions

No.	Distance from symmetry plane (mm)	Outer diameter (mm)		Inner diameter (mm)				
		Measured value		Measured value				Average value
1	60	7.06	7.02	2.12	2.16	2.36	2.26	2.225
2	50	7.16	7.16	2.10	2.22	2.22	2.34	2.22
3	40	7.08	7.06	2.14	2.06	2.02	2.02	2.06
4	30	7.00	6.98	1.88	1.92	1.96	1.98	1.935
5	20	7.00	7.00	1.88	2.04	1.96	2.08	1.99
6	10	7.04	6.98	2.36	2.40	2.30	2.36	2.355
7	0	7.04	7.02	2.24	2.28			2.26
8	10	7.06	7.02	Max 7.16 (outer), min 6.88 (outer); average 2.14 (inner)				
9	20	6.88	6.88					
10	30	7.00	6.98					
11	40	7.1	7.06					
12	50	7.04	7.00					
13	60	7.00	7.00					

Condition 2: α=35°, stretching angle at the knifing zone β=5°, and stretching angle at the stretching zone β=4°. The quality of the workpiece improved greatly. The diameter of the workpiece section was measured; the original size was 12 mm×6 mm, and the diameter of the theoretical rolling was 7 mm. Figure 7b shows the measured section. The diameters of the measurement data are shown in Table 5. The measurement results show that the difference between the minimum inner diameter at the center plane of symmetry and the average inside diameter of the other plane is 0.325 mm. The difference between the minimum and the maximum outer diameters of the theoretical diameter is less than 3 %, which indicates that the data are acceptable and that the parameters are satisfactory.

Condition 3: α=35°, stretching angle at the knifing zone β=6.5°, and stretching angle at the stretching zone β=6°. In this condition, the #45 steel is triangular, whereas 4Cr9si2 has serious ovalization fracture and cannot be formed.

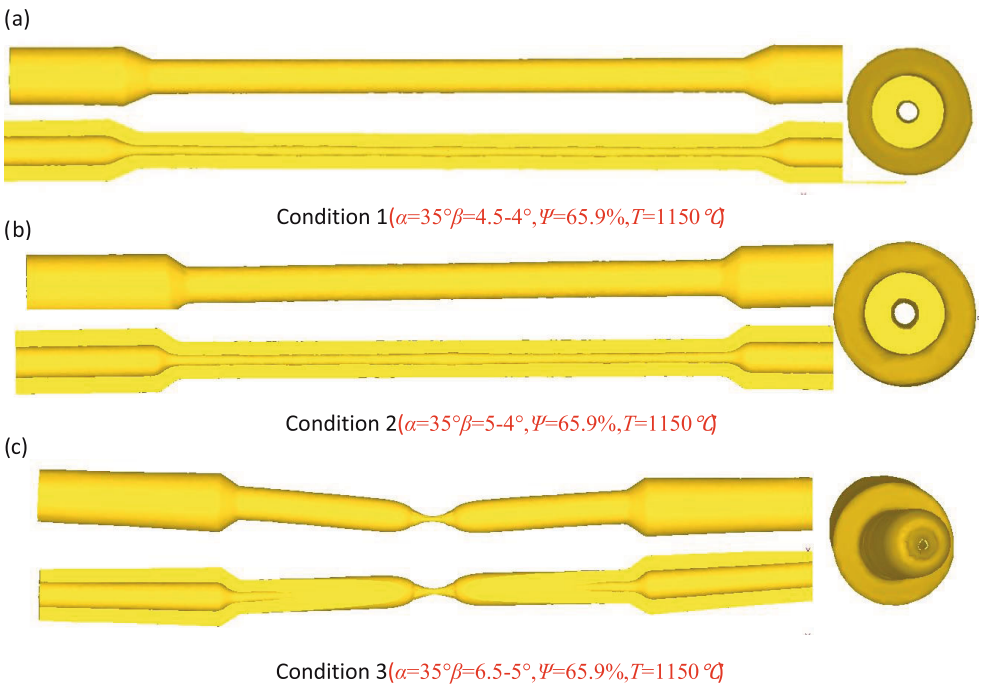

Fig. 9 Rolled billets in different conditions

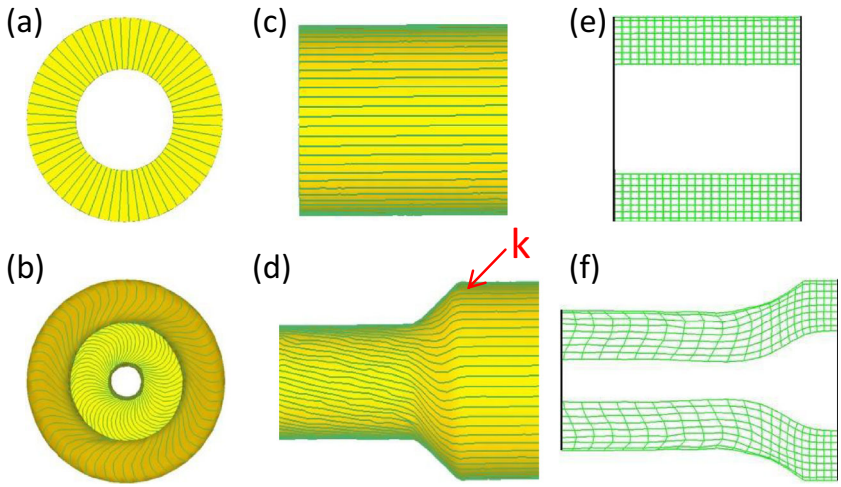

Fig. 10 The deformation grid during the CWR hollow valve process. **a** The initial lateral grid. **b** The lateral grid after deformation. **c** The initial longitudinal grid. **d** The longitudinal grid after deformation. **e** The initial longitudinal single-layer grid. **f** The longitudinal single-layer grid after deformation

3.2 FEM results

This study utilized the DEFORM software based on the FEM. The DEFORM software may be used in the mechanical or thermomechanical simulation of metal forming processes. The three conditions described above were simulated (Fig. 9).

Condition 2 was selected based on the experiment results. DEFORM was used to precisely track the material flow mechanisms, the temperature distributions, and the strain and rolling force values.

3.2.1 Material flow

The primary deformation of the workpiece is radially compressed and axially extends the wall thinning. Figure 10a shows the initial lateral grid. Figure 10b shows the lateral grid after deformation. The material shows considerable twisting in the rotational direction. The twisting degree grows from the inner wall to the outer wall of the roll. Figure 10c shows the initial longitudinal grid. Figure 10d shows the longitudinal grid after deformation. The workpiece twists, and the degree of twisting increases gradually. From the rolling contact zone to the center of the symmetry section, the twisting of the mesh increases gradually. The direction of the twisting of the mesh is similar to the rotational direction of the roll. In the upper part of the rolling contact surface, the direction of the twist is opposite the rolling direction. There is a position that does not twist. The position of the rolling member and the mold is not relative to the sliding contact point K. At this position, the rolling member and the die must have the same line velocity. Below the rolling position of point K, the line speed of the mold is greater than the linear velocity of the rolling member. The line speed of the surface member subjected to friction is faster than the rotating speed. These conditions lead to the reversal of the rolling direction. Above the rolling position of point K, the mold line speed is less than the line speed of the rolling member. The line speed of the surface member subjected to friction is lower than the rotating speed. The direction of the twist is opposite the rotational direction.

Figure 10e shows the initial longitudinal single grid, and Fig. 10f shows the single longitudinal grid after deformation. The parallel element mesh deformation also occurs. The axial flow of the material increases from the inner wall to the outer wall, and the difference increases as rolling length increases. Therefore, axial inhomogeneous deformation is significant in the CWR of hollow parts. Uneven deformation and local deformation are mainly attributed to surface friction.

3.2.2 Temperature

In the CWR process, the temperature of the workpiece increases because of heat deformation. Heat exchange with the environment causes the temperature to drop [26, 29]. To analyze the rolling temperature, four roll cross sections (from the neutral planes measuring 0, 5, 15, and 25 mm) were selected for this study. Four points (whose sequential rolling surfaces point toward the center) were selected for analysis (Fig. 11). The location of the points were presented in Fig. 11e. As shown in Fig. 11a, b, points 4 and 8 at the knifing zone come in contact with mold surface, causing the temperature to decrease rapidly and reach a minimum of about 1040 °C. The outer surface temperature at the stretching zone reaches 1100 °C. Figure 11c shows a temperature of about 1030 °C. The lowest temperature occurs at 2.45 s. Figure 11d shows that the temperature does not sharply drop because of the lack of mold surface contact. With the completion of the rolling process, the temperature in the rolling section decreases to 1080 °C. As plasticity is favorable within this temperature range, rolling is easy. A similar temperature difference was also observed through infrared thermography in the experimental tests (Fig. 12). Figure 12a

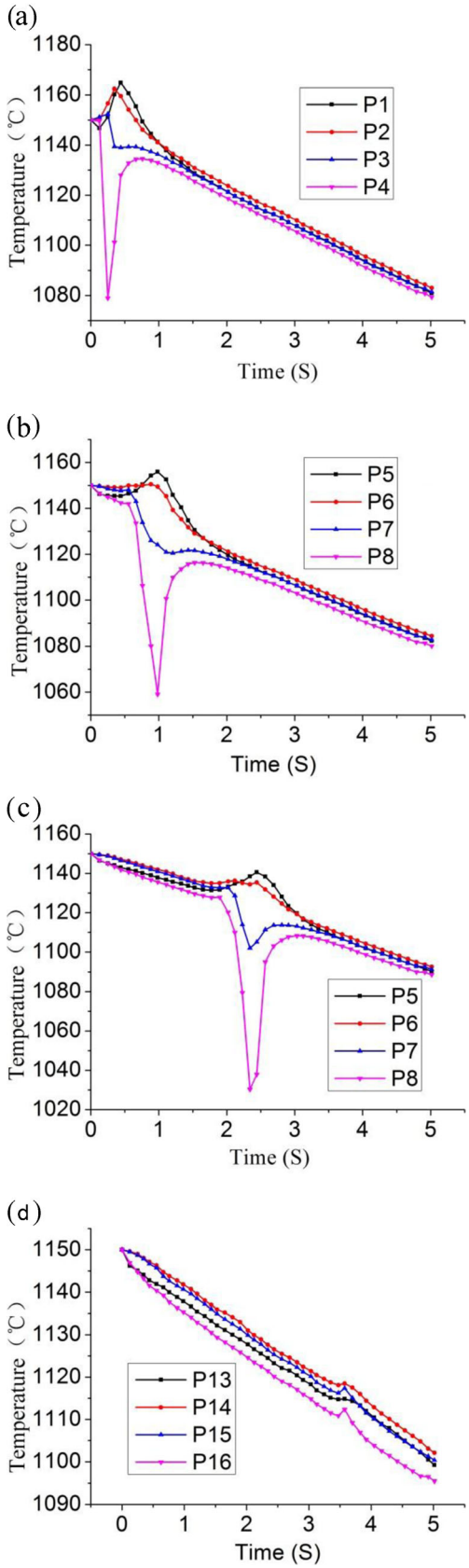

Fig. 11 The temperature distribution of the CWR hollow valve process

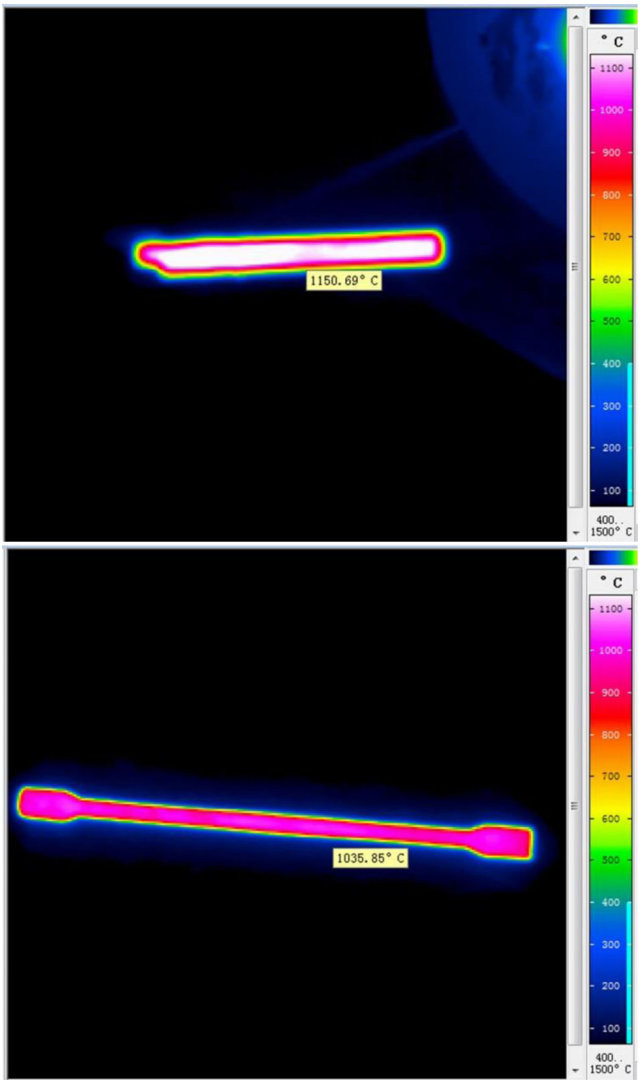

Fig. 12 Photograph recorded using infrared thermography shows the temperature distribution during the CWR hollow valve process

depicts the temperature of the billet before rolling. Figure 12b demonstrates the temperature of the billet after rolling.

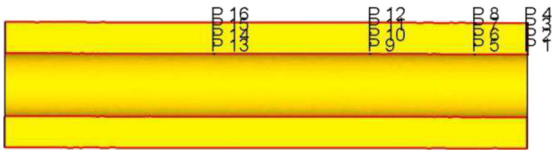

3.2.3 Strain

To analyze the rolling strain, two points (inner point P1 and surface point P2) were selected for this study. Figure 13 shows the distribution of the strain. Initially, the radial strain, as well as the axial and tangent strains, is a tensile strain. After entering the rolling deformation zone, the radial strain alternates between the tensile strain state and the compressive strain state. The value increases quickly and then fluctuates.

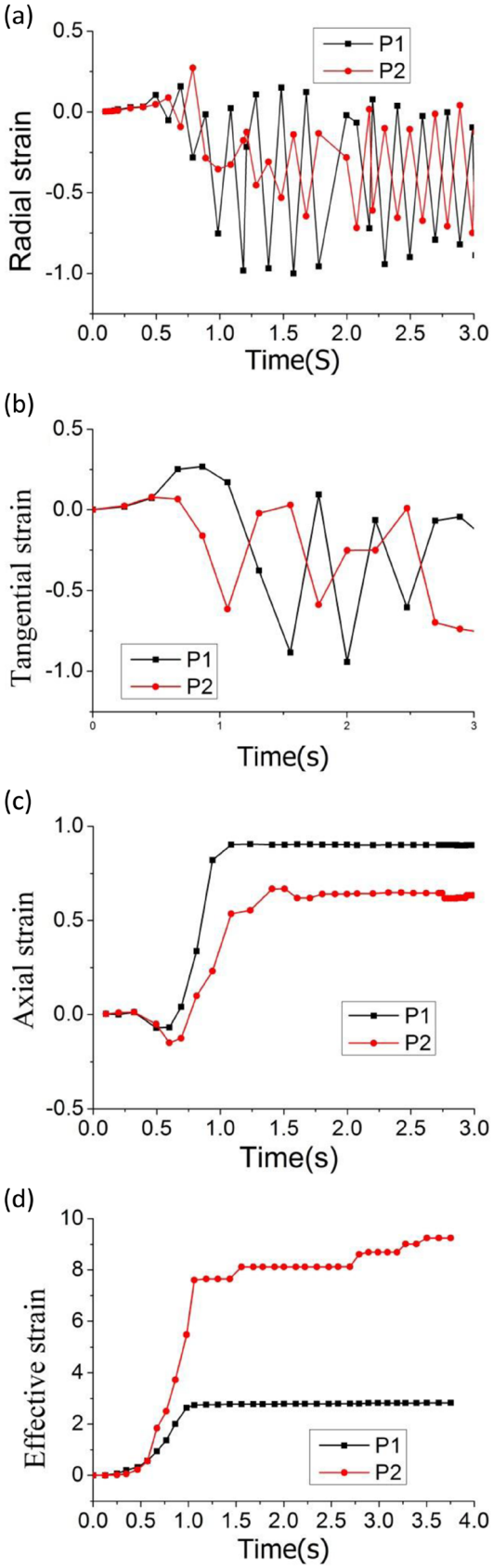

Fig. 13 The strain distribution of the CWR hollow valve process

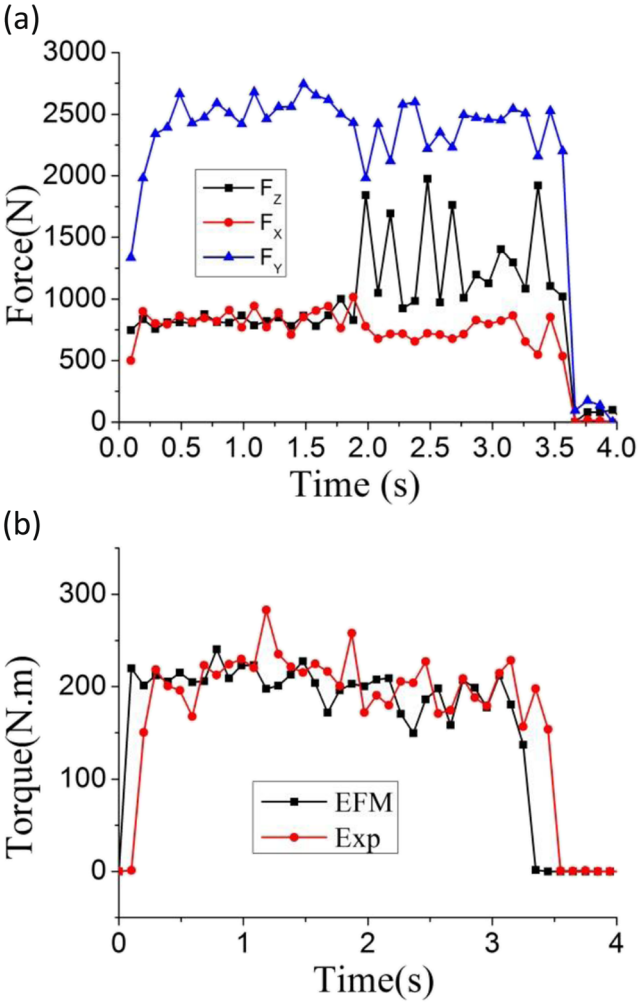

Fig. 14 The distribution of forces and torque

The strain in the inner point is greater than that in the surface point. Meanwhile, tangent strain shows a greatly different value. The strain in the inner point shows greater fluctuation than that in the surface point. Axial strain is a tensile strain in the deformation process.

As shown in Fig. 13d, which depicts the effective strain distribution of the CWR process, the strain in the surface point

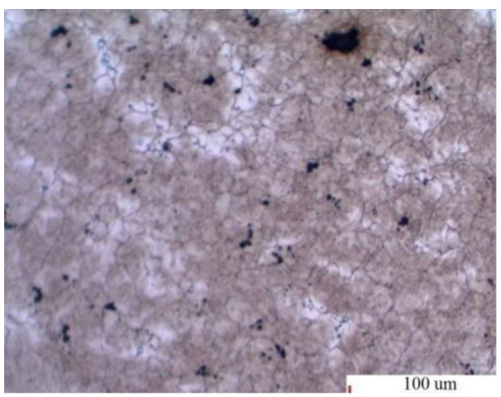

Fig. 15 The grain size under 1150 °C (16.5 um)

Fig. 16 Experiment and simulation of CWR hollow valve

changes faster than that in the inner point. The deformation of the surface is large. After entering the sizing area, the strain reaches a stable value. In a summit, strain rapidly increases in the deformation zone, and the radial and tangent strains undergo periodic fluctuations. In the end, tangent strain is gradually stabilized.

3.2.4 Rolling force

Determining the rolling forces and rolling torque is greatly important. The rolling force is the main basis for the rolling mill design, whereas the rolling torque is the main basis for the calculation of motor power [1, 25]. Steel valve has high deformation resistance and thus requires a large amount of energy for forging. Therefore, analyzing the rolling force and rolling torque at different time points is necessary. Figure 14a presents the distribution of forces of the influencing tools during the CWR process. This figure shows how forces change. According to the data in Fig. 14a, the distribution of forces is qualitatively almost identical; however, the quantitatively radial force is three times greater than the tangent force. The radial force is about 2500 N while the tangent force is about 750 N. Axial force is similar to tangent force.

Figure 14b presents a comparison between the torque measured in the experiments and calculated in the simulation during the CWR process. The distribution of the rolling torque is shown in the figure. Torque is relatively stable and volatile. The average torque is 300 N m in the process.

The numerical calculations indicate the possibility of forming 4Cr9Si2 hollow valves with a small diameter. The results of the experiment and simulation of the CWR forces are in good agreement. The FEM can be successfully used to evaluate forming quality, where the knowledge of which is necessary for the proper design of CWR processes. In future research, we can use this modeling to predict the formation of hollow valves for industrial production.

4 Industrial application

Figure 15 presents the microstructure of the valve stem at 1150 °C. The 4Cr9Si2 martensitic steel rolling grains are basically isometric after rolling. The grains do not show obvious elongation or recrystallization. All the rolled grains undergo dynamic recrystallization and thus meet the grain size requirements of the valve. Figure 16 shows the hollow valve after rolling in both the experiment and the simulation. The original diameter is 12 mm × 6 mm. After rolling, the diameter is 7 mm. The actual rolling is 7.05 mm (average), and the FE simulation result is 6.87 mm. The experiment and simulation of CWR show good agreement. Therefore, using CWR to produce hollow valves is feasible.

5 Summary and conclusions

Systematic studies were conducted on hollow valves produced via CWR. The experiments and numerical analyses led to the following conclusions:

1. Producing a 4Cr9Si2 hollow valve with a small diameter via CWR is feasible.
2. Changing the stretching angle (β) could solve the problem of a swollen hole.
3. Forming angle (α) and stretching angle (β) are important parameters for the CWR process. When the forming angle (α) is equal to 35° and the stretching angle (β) is equal to 5° and 4° in the knifing zone and stretching zone, respectively, the forming quality of the workpiece can be greatly improved.
4. The Kumar model was used to establish the constitutive equations, and DEFORM was utilized to precisely track the material flow mechanisms, temperature distributions, and strain and rolling force values.
5. Grain microstructure was analyzed. The valve meets the production standard. Thus, CWR has a great advantage in valve production.

Acknowledgments The authors would like to gratefully acknowledge the support of Guangdong Province Dengyun Auto Parts academician workstation roll forming of new technologies (No. 2011A090700026)

References

1. Hu ZH, Zhang KS, Wang BY, Shu XD (2004) Formed technology and simulation of parts about the cross-wedge rolling. Publ House Metall Ind Beijing 1–10:180–185
2. Liu JP, Hu ZH, Long SX. An automobile engine valve blank precise forming method with cross wedge rolling: China Patent, 201010107843.3. 2010-7-28
3. Shu XD, Li CM, Zhao J, Hu ZH (2007) Theoretical and experimental study of varying rule of rolling-moment about cross-wedge rolling. J Mater Process Technol 187–188:752–756
4. Zhao J, Shu XD, Hu ZH (2005) Study of stress distribution of forming slandering of automobile semi-axes with multi-wedge rolling by FEM simulation. ICMIT 2005: Control systems and robotics, Pts 1 and 2 6042: 4247–4247
5. Zhao J, Lu LQ, Hu ZH (2007) Study on varying rule of mechanical parameters in forming automobile semi-axes with multi-wedge cross wedge rolling. Proc Int Conf Mech Eng Mech 2007 1-2:1723–1727

6. Pater Z (2006) Finite element analysis of cross wedge rolling. J Mater Process Technol 173:201–208
7. Pater Z (2000) Theoretical and experiment analysis of cross wedge rolling process. Int J Mach Tools Manuf 40:49–60
8. Pater Z (1999) Numerical simulation of the cross wedge rolling process including upsetting. J Mater Process Technol 92–93:468–473
9. Li Q, Lovell MR (2008) Cross wedge rolling failure mechanism and industrial application. Int J Adv Manuf Technol 37:265–278
10. Li Q, Lovell MR (2002) Predicting critical friction in a two-roll cross wedge rolling process. J Tribol 125:200–203
11. Li Q, Lovell MR (2004) The establishment of a failure criterion in cross wedge rolling. Int J Adv Manuf Technol 24:180–189
12. Li Q, Lovell MR (2005) On the critical interfacial friction of a two roll CWR process. J Mater Process Technol 160:245–256
13. Zhou J, Chuan X, Ying YY, Jia Z (2013) Influence of tool parameters on tool wear in two-roll cross-wedge roll. Int J Adv Manuf Technol 65:745–753
14. Zhou J, Yu YY, Zeng Q (2014) Analysis and experimental studies of internal voids in multi-wedge cross wedge rolling stepped shaft. Int J Adv Manuf Technol. doi:10.1007/s00170-014-5768-9
15. Zhou J, Jia Z, Ji JJ, Yu YY, Xiao C (2012) Influence of tool parameters on internal voids in cross wedge rolling of aluminum alloy parts. Trans Nonferrous Metals Soc China 22:s21–s26
16. Wang MH, Xiang D, Xiao C, Zhou J, Jia Z (2012) Influence of cooling condition of tools on central deformation of workpiece and tool wear in cross wedge rolling. Int J Adv Manuf Technol 59:473–482
17. Bartnicki J, Pater Z (2005) Numerical simulation of three-rolls cross-wedge rolling of hollowed shaft. J Mater Process Technol 164–165: 1154–1159
18. Bartnicki J, Pater Z (2004) The influence of tool geometry on the CWR process of hollowed shafts. Steel Grips J Steel Relat Mater 2: 103–107, Suppl. metal forming
19. Urankar S, Lovell M, Morrow C, Li Q, Kawada K (2006) Establishment of failure conditions for the cross-wedge rolling of hollow shafts. J Mater Process Technol 177:545–549
20. Urankar S, Lovell M, Morrow C, Li Q, Kawada K (2006) Development of a critical friction model for cross wedge rolling hollow shafts. J Mater Process Technol 177:539–544
21. Wang MT, Li XT, Du FS (2005) A coupled thermal–mechanical and microstructural simulation of the cross wedge rolling process and experimental verification. Mater Sci Eng A 391:305–312
22. Li XT, Wang MT, Du FS (2006) The coupling thermal–mechanical and microstructural model for the FEM simulation of cross wedge rolling. J Mater Process Technol 172(2):202–207
23. Wang MT, Li XT, Du FS, Zheng YZ (2004) Hot deformation of austenite and prediction of microstructure evolution of cross-wedge rolling. Mater Sci Eng A 379(1–2):133–140
24. Wang JM, Zhu XZ, Cui HJ, Wang J (2011) Study on damage of hollow shafts rolled by cross-wedge rolling. Hot Work Technol 40:97–100
25. Wang JM, Yu KF, Hu M, Zhu HY, Gong GC (2008) Simulation of hollow shafts rolled by cross wedge rolling and regularity of wall thickness change. Hot Work Technol 37:73–77
26. Zhang N, Wang BY, Hu ZH (2011) Thermomechanical coupled numerical simulation of GH4169 alloy for cross wedge rolling. J Univ Sci Technol Beijing 33:1396–1401
27. Ning YQ, Fu MW, Chen X (2012) Hot deformation behavior of GH4169 superalloy associated with stick δ phase dissolution during isothermal compression process. Mater Sci Eng A 540:164–173
28. Lin YC, Chen XM, Wen DX, Chen MS (2014) A physically-based constitutive model for a typical nickel-based superalloy. Comput Mater Sci 83:282–289
29. Ying FQ, Pan BS (2007) Analysis on temperature distribution in cross wedge rolling process with finite element method. J Mater Process Technol 187–188:392–396
30. Tang GB, Liu ZD, Kang YL, Wang W, Zhang PJ (2006) Simulation of thermal evolution of strip and determination of heat transfer coefficient in deformation zone during hot rolling. Iron Steel 41(5):36–40
31. Xing L, Zhang LW, Zhang XZ (2009) Effect of temperature and load on contact heat transfer between GH4169 and 5CrMnMo. J Cent South Univ Sci Technol 40(6):1568–1572